Dynamic response of aerospace structures by means of refined beam theories

Dynamic response of aerospace structures by means of refined beam theories

A. Pagani[*], M. Petrolo[†], G. Colonna[‡], E. Carrera[§]

Department of Mechanical and Aerospace Engineering, Politecnico di Torino,
Corso Duca degli Abruzzi 24, 10129 Torino, Italy.

Submitted to

Aerospace Science and Technology

Revised version of the AESCTE-D-15-00492 paper

Author for correspondence:
E. Carrera, Professor of Aerospace Structures and Aeroelasticity,
Department of Mechanical and Aerospace Engineering,
Politecnico di Torino,
Corso Duca degli Abruzzi 24,
10129 Torino, Italy,
tel: +39 011 090 6836,
fax: +39 011 090 6899,
e-mail: erasmo.carrera@polito.it

[*]Research Fellow, e-mail: alfonso.pagani@polito.it
[†]Research Fellow, e-mail: marco.petrolo@polito.it
[‡]Graduate student, e-mail: giovanni.colonna@polito.it
[§]Professor of Aerospace Structures and Aeroelasticity, e-mail: erasmo.carrera@polito.it

Abstract

The present paper is devoted to the investigation of the dynamic response of typical aerospace structures subjected to different time-dependent loads. These analyses have been performed using the mode superposition method combined with refined one-dimensional models, which have been developed in the framework of the Carrera Unified Formulation (CUF). The Finite Element Method (FEM) and the principle of virtual displacements are used to compute the stiffness and mass matrices of these models. Using CUF, one has the great advantage to obtain these matrices in terms of fundamental nuclei, which depend neither on the adopted class of beam theory nor on the FEM approximation along the beam axis. In this paper, Taylor-like expansions (TE), Chebyshev expansion (CE) and Lagrange expansion (LE) have been employed in the framework of CUF. In particular, the latter class of polynomials has been used to develop pure translational displacement-based refined beam models, which are referred to as Component Wise (CW). This approach allows to model each structural component as a 1D element. The dynamic response analysis has been carried out for several aerospace structures, including thin-walled, open section and reinforced thin-shells. The capabilities of the proposed models are demonstrated, since this formulation allows to detect shell-like behaviour with enhanced performances in terms of computational efforts.

Keywords: Refined beam theories, Finite elements, Carrera unified formulation, Dynamic response, Mode superposition.

1 Introduction

In aerospace engineering applications, several types of slender structures are used. For example, aircraft wings and fuselages, rotor and wind blades, launchers and rockets can be modeled as one-dimensional (1D) structures. Thus, these components can be analyzed using beam assumptions and 1D approaches, which have the great advantage to require lower computational costs than bi-dimensional (2D) plate and shell models or 3D solid models [1]. The beam models referred to as classical are the Euler-Bernoulli Beam Theory (EBBT) [2], in which the transverse shear deformation is neglected, and the Timoshenko Beam Theory (TBT) [3, 4], which assumes a constant shear strain across the section. However, several problems (e.g., short beams and composite structures) require to overcome these assumptions since their use can lead to incorrect results.

Over the years, much effort has been done in order to improve and refine the classical beam theories [5, 6, 7, 8]. These works aimed to compute a suitable shear correction factor for several cases: torsional and flexural shearing stresses in prismatic beams, arbitrary shaped cross-sections, wide, thin-walled and bridge-like structures. A second order beam theory which takes into account shear curvature, transverse direct stresses and rotatory inertia was presented in [9], whereas a theory for beams of rectangular cross-section capable to include the warping effects of the cross-sections was presented by Levinson [10]. Levinson's theory was then extended to two-dimensional linear theory of elasticity in [11]. An overview of models adopted for the analysis of laminated beams and plates, with particular emphasis on vibrations and wave propagation, was given in [12]. In [13], the finite element formulation for a variationally consistent higher-order beam theory was presented for the static and dynamic behavior of rectangular beams, whereas in [14] static and free vibration analyses were performed using a higher-order shear-deformable beam model. A refined theory suitable for the static and/or dynamic analysis of an orthotropic straight beam was developed in [15], whereas Marur proposed three higher-order refined displacement models in [16]. Moreover, the vibrations of angle ply laminated beams were studied using a higher-order theory and isoparametric 1D finite element formulations in [17]. The analytical solution to the natural frequency analysis of composite and sandwich beams based on a higher-order refined theory was presented in [18]. In [19], an analytic solution for free and forced vibrations of stepped Timoshenko beams was presented. This solution was used for the approximate analysis of generally non-uniform Timoshenko beams, whereas Librescu and Na [20] dealt with the problem of controlling the bending oscillations of cantilevers subjected to harmonic time-dependent excitations. Moreover, a procedure for the enhancement of the response characteristic of the proposed models was presented in the same work. Ould Larbi et al. [21] recently developed a shear deformation beam theory based on neutral surface position for bending and free vibration analysis of functionally graded beams. 3D elasticity equations were reduced to a beam-like formulation by Ladevze [22, 23, 24], obtaining a solution for high aspect-ratio thin-walled beams. Berdichevsky [25] proposed asymptotic type expansions based on variational methods. This method was further developed in the VABS models presented by Volovoi [26], Volovoi and Hodges [27], Popescu and Hodges [28], Yu and Hodges [29, 30]. Subramanian [31] carried out the free vibration analysis of laminated composite beams using

finite elements based on two higher-order displacement-based shear deformation theories. Moreover, in [32], the investigation of the free undamped vibration response of tapered composite beams, using a higher-order finite element formulation, was carried out. Şimşek and Kocatürk [33] studied the free vibration of beams with different boundary conditions within the framework of the third-order shear deformation theory. For further details about modern models for beam structures and a comprehensive review, the reader is referred to [34].

In the aforementioned papers, the theories developed are problem dependant. This means that, different problems may require the adoption for different models. The present paper adopts a refined 1D model that can be employed independently on the problem characteristics and complexity. Those refined beam models are developed in the framework of the Carrera Unified Formulation (CUF), a hierarchical approach which has been developed initially for plates and shells [35, 36] and then extended to beams [37, 38]. The hierarchical formulation of CUF models enables the arbitrary choice of the expansion functions over the cross-section up to the desired order [39]. Thus, any-order structural models can be implemented with no need of formal changes in the problem equations and matrices. The use of a CUF model allows to deal with arbitrary geometries, boundary conditions and material configurations with no need of ad hoc formulations. CUF capabilities combined with the simplicity of 1D models allow to detect shell- and solid-like solutions for either static [40], free-vibration [41, 42, 43, 44] and buckling [45] analyses. In [46], the dynamic response of thin-walled structures has been investigated combining CUF beam theories with the Newmark method. The aforementioned works have been performed by means of Taylor-like Expansion (TE). On the other hand, in [47] the displacement field across the section was modeled by means of Lagrange Expansion (LE) polynomials, whereas a beam theory based on Chebyshev Expansion (CE) polynomials has been introduced in [48]. The LE models have the great advantage of considering only pure displacement variables, enabling the use of the Component-Wise (CW) approach. This approach allows the representation of every component of the structure through a 1D CUF model, i.e. the same 1D finite element is used for each part of the structure. This characteristic is of particular interest for the modelling of multi-component constructions, such as aircraft reinforced-shells. In classical approaches, in fact, by mainly using the direct stiffness method, each component of the aircraft structure (e.g., panels and stiffeners) are modelled separately by using 1D and 2D finite elements. These elements are then assembled or, if appropriate, linked together by using fictitious multi-point constrains, which introduce some physical inconsistencies in the mathematical formulations (see [49]). On the other hand, only the real surfaces of the structure are used to formulate the mathematical FE model in the CW approach. In [50], the CW approach was recently used to study laminated anisotropic composites, whereas typical aerospace structures have been analyzed in [49] and [51].

The present research mainly deals with dynamic response problems, which are of great interest for lifting systems in unsteady dynamic pressure fields [52], for loads deriving from sonic shock-waves [53] and for launches and impacts, which cause impulsive loadings on the structure [54]. A typical aerospace structure is

often subjected to loads originating from sudden, abrupt or constant gravity accelerations. Thus, inertial and dynamic loads must be taken into account. A typical dynamic load is a gust. Gust loadings affect different aspect of the aircraft design and operation, playing a key role in dynamic load, flight stability, safety and control fields. The gust structure is defined as turbulence when it is characterised by a random nature and a velocity profile that tends to be continuous and irregular. On the other hand, when it consists of more or less isolated pulses, the single pulse is referred to as a gust [55]. In this work, the approach adopted in [56, 57] is considered and the time-history response to gust is analyzed. Although in principle the solution to dynamic problems could be obtained by standard procedures, in practical a greater interest is addressed towards few effective numerical methods, which fall within direct integration and mode superposition categories. In the first case (e.g., central difference, Houbolt, and Newmark methods), a numerical step-by-step procedure [1, 46] is adopted. However, as a main drawback, these procedures require large computational times and are affected by possible instability due to error growth. On the other hand, several works have adopted the mode superposition to investigate the dynamic response of structures [1]. For example, in [58] this approach was adopted for the analysis of nonlinear dynamic problems involving impacts, whereas a technique for the approximate solution of nonlinear initial-boundary-value problems of structural dynamics was proposed in [59]. Moreover, modal frequency response analysis was performed in [60] by means of an improved mode-superposition technique, whereas the transient dynamic response of composite and sandwich plates was investigated by means of a refined shear deformation theory and mode superposition technique in [61].

The use of refined 1D models is relevant to predict the time-dependent response of thin-walled slender structures, as those considered in [62]. In this paper, 1D CUF is employed along with mode superposition method to conduct dynamic response analysis on various structures. First, a simply supported beam subjected to a harmonic load is considered. Then, thin-walled aerospace structures subjected to harmonic and distributed loads and wing-like structures subjected to harmonic and pulse gust loads are investigated. This paper is organized as follows: classical beam theories are presented in Section 2 , whereas Section 3 gives an overview of the higher-order beam theories developed in the framework of CUF. Section 4 gives a brief outline of the FEM approach and gives an overview of the mode superposition method, whereas in Section 5 the extension of inertial and pulse gust loads in the framework of CUF is briefly presented. Subsequently, in Section 6 the results obtained using the proposed CUF theories are discussed. Section 7 is devoted to the conclusions.

2 Classical beam theories

Figure 1 shows the Cartesian coordinate system adopted for a generic beam structure. The cross-section Ω is normal to the beam axis y, which has boundaries $0 \leq y \leq L$. It should be highlighted that the validity of the proposed formulation is not affected by the shape of the cross-section and the rectangular cross-section adopted

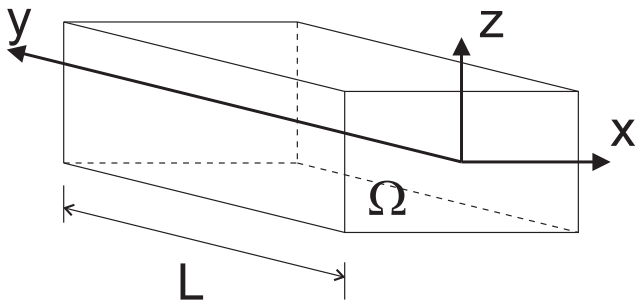

Figure 1: Coordinate frame of the beam.

has merely explicative purposes. According to the Euler-Bernoulli Beam Theory (EBBT), the kinematic field is

$$\begin{aligned} u_x(x,y,z) &= u_{x1}(y) \\ u_y(x,y,z) &= u_{y1}(y) - x\,\frac{\partial u_{x1}(y)}{\partial y} + z\,\frac{\partial u_{z1}(y)}{\partial y} \\ u_z(x,y,z) &= u_{z1}(y) \end{aligned} \tag{1}$$

where u_x, u_y and u_z are the displacement components of a point along x, y and z axes, respectively; u_{x1}, u_{y1} and u_{z1} are the displacements of the beam axis whereas $-\frac{\partial u_{x1}}{\partial y}$ and $\frac{\partial u_{z1}}{\partial y}$ are the rotations of the cross-section about the z-axis (i.e. ϕ_z) and x-axis (i.e. ϕ_x). In EBBT, the cross-sectional shear deformation phenomena are neglected. Therefore, the deformed cross-section is assumed plane and orthogonal to the beam axis. An improved displacement field is adopted in the Timoshenko Beam Theory (TBT)

$$\begin{aligned} u_x(x,y,z) &= u_{x1}(y) \\ u_y(x,y,z) &= u_{y1}(y) + x\,\phi_z(y) - z\,\phi_x(y) \\ u_z(x,y,z) &= u_{z1}(y) \end{aligned} \tag{2}$$

Since the the cross-section does not necessarily remain perpendicular to the beam axis after deformation and the original displacement field is enriched by the unknown rotations, ϕ_z and ϕ_x, it is clear that TBT constitutes an improvement over EBBT. For a comprehensive review about classical and modern 1D modelling techniques, the reader is referred to [34].

3 Higher-order, hierarchical models by CUF

Considering slender, solid-section, homogeneous structures subject to bending phenomena, classical beam models provide a reasonably good approximation of the problem. On the other hand, more sophisticated theories are needed in case of short, thin-walled, open cross-section beam analyses. These theories adopt richer kinematic fields to obtain more accurate 1D models. The Carrera Unified Formulation (CUF) can be used to develop refined beam models having an arbitrary number of terms in the kinematic field. In the

framework of the CUF, the kinematics of a beam model can be summarized as follows:

$$\mathbf{u}(x,y,z) = F_\tau(x,z)\mathbf{u}_\tau(y), \qquad \tau = 1,2,....,M \tag{3}$$

where $\mathbf{u}(x,y,z) = u_x(x,y,z)u_y(x,y,z)u_z(x,y,z)^T$ is the displacement vector; F_τ indicates the functions of the cross-section coordinates x and z; $\mathbf{u}_\tau$ is the generalized displacement vector; M indicates the number of terms in the expansion. It should be noted that the repeated subscript indicates summation. Moreover, the choice of F_τ and M is arbitrary. Thus, the basis functions adopted to model the displacement field across the section can be different and expanded to any order. The models known in the literature as TE (Taylor Expansion) [38, 63, 43] are obtained considering Taylor-like expansion polynomials as F_τ functions. For example, the displacement field of the second-order TE model can be expressed as follows:

$$\begin{aligned}
u_x(x,y,z) &= u_{x_1}(y) + x\ u_{x_2}(y) + z\ u_{x_3}(y) + x^2\ u_{x_4}(y) + xz\ u_{x_5}(y) + z^2\ u_{x_6}(y) \\
u_y(x,y,z) &= u_{y_1}(y) + x\ u_{y_2}(y) + z\ u_{y_3}(y) + x^2\ u_{y_4}(y) + xz\ u_{y_5}(y) + z^2\ u_{y_6}(y) \\
u_z(x,y,z) &= u_{z_1}(y) + x\ u_{z_2}(y) + z\ u_{z_3}(y) + x^2\ u_{z_4}(y) + xz\ u_{z_5}(y) + z^2\ u_{z_6}(y)
\end{aligned} \tag{4}$$

where the parameters on the right-hand side (u_{x_1}, u_{y_1}, u_{z_1}, u_{x_2}, etc.) represent the components of the generalized displacement vector. Other classes of hierarchical CUF models adopt the Lagrange polynomials and the Chebyshev polynomials as F_τ functions. These models are referred to as Lagrange Expansion (LE) and Chebyshev Expansion (CE) models, respectively. The CE second-order kinematic model with 18 generalized displacement variables can be defined as follows:

$$\begin{aligned}
u_x(x,y,z) &= P_{00}(x,z)u_{x_1}(y) + P_{10}(x,z)u_{x_2}(y) + P_{01}(x,z)u_{x_3}(y) + P_{20}(x,z)u_{x_4}(y) + P_{11}(x,z)u_{x_5}(y) + P_{02}(x,z)u_{x_6}(y) \\
u_y(x,y,z) &= P_{00}(x,z)u_{y_1}(y) + P_{10}(x,z)u_{y_2}(y) + P_{01}(x,z)u_{y_3}(y) + P_{20}(x,z)u_{y_4}(y) + P_{11}(x,z)u_{y_5}(y) + P_{02}(x,z)u_{y_6}(y) \\
u_z(x,y,z) &= P_{00}(x,z)u_{z_1}(y) + P_{10}(x,z)u_{z_2}(y) + P_{01}(x,z)u_{z_3}(y) + P_{20}(x,z)u_{z_4}(y) + P_{11}(x,z)u_{z_5}(y) + P_{02}(x,z)u_{z_6}(y)
\end{aligned} \tag{5}$$

The above model is analogous to the second-order TE model since it involves three constant variables, six linear and nine parabolic terms.

In LE models, the unknown variables are only pure displacements. This formulation allows one to adopt a Component-Wise (CW) approach [50, 49, 51]. Lagrange elements are in fact used to model the displacement variables in each structural component, whereas arbitrary geometry can be set adopting the iso-parametric formulation. In this work, mainly bi-quadratic nine-nodes (L9) Lagrange polynomials are used as F_τ. Lagrange polynomials can be found in [47]. The displacement field within a L9 element can be written as:

$$\begin{aligned}
u_x(x,y,z) &= F_1(x,z)u_{x1}(y) + F_2(x,z)u_{x2}(y) + ... + F_9(x,z)u_{x9}(y) \\
u_y(x,y,z) &= F_1(x,z)u_{y1}(y) + F_2(x,z)u_{y2}(y) + ... + F_9(x,z)u_{y9}(y) \\
u_z(x,y,z) &= F_1(x,z)u_{z1}(y) + F_2(x,z)u_{z2}(y) + ... + F_9(x,z)u_{z9}(y)
\end{aligned} \tag{6}$$

where $u_{x1}, ..., u_{z9}$ are the translational components of the nine points of the L9 element. In classical approaches, each component of multi-component structures is modeled in relation with their geometry and scale. On the other hand, CW allows the representation of every part through a 1D CUF model, leading to the use of the same 1D finite element, i.e. the same stiffness matrix in the FEM framework. For more details about the CW approach and the features of LE models, the reader is referred to [50, 64, 65], whereas a detailed dissertation of the CE models can be found in [48].

4 Finite element formulation

In this paper, FEM has been used to formulate the undamped free vibration problem in the framework of 1D CUF. Subsequently, the modal shapes obtained from free vibration analyses have been used with reference to the mode superposition method to investigate the dynamic forced response of the proposed models. A brief overview of the FEM when applied to CUF is given in the following section, whereas the mode superposition method is introduced in Section 4.3.

4.1 Preliminaries

The stress σ and the strain ϵ vectors are defined as follows:

$$\begin{aligned} \boldsymbol{\sigma} &= \{\sigma_{yy}, \sigma_{xx}, \sigma_{zz}, \sigma_{xz}, \sigma_{yz}, \sigma_{xy}\}^T \\ \boldsymbol{\epsilon} &= \{\epsilon_{yy}, \epsilon_{xx}, \epsilon_{zz}\epsilon_{xz}, \epsilon_{yz}, \epsilon_{xy}\}^T \end{aligned} \tag{7}$$

In the case of small displacements, the following relation between strains and displacements holds:

$$\boldsymbol{\epsilon} = \boldsymbol{D}\boldsymbol{u} \tag{8}$$

where the linear differential operator $\boldsymbol{D}$ is defined as follows:

$$\boldsymbol{D} = \begin{bmatrix} 0 & \frac{\partial}{\partial y} & 0 \\ \frac{\partial}{\partial x} & 0 & 0 \\ 0 & 0 & \frac{\partial}{\partial z} \\ \frac{\partial}{\partial z} & 0 & \frac{\partial}{\partial x} \\ 0 & \frac{\partial}{\partial z} & \frac{\partial}{\partial y} \\ \frac{\partial}{\partial y} & \frac{\partial}{\partial x} & 0 \end{bmatrix} \tag{9}$$

The constitutive law can be used to obtain the stress components:

$$\boldsymbol{\sigma} = \tilde{\boldsymbol{C}}\boldsymbol{\epsilon} \tag{10}$$

Considering an isotropic material, $\tilde{\boldsymbol{C}}$ can be written as:

$$\tilde{\boldsymbol{C}} = \begin{bmatrix} \lambda+2G & \lambda & \lambda & 0 & 0 & 0 \\ \lambda & \lambda+2G & \lambda & 0 & 0 & 0 \\ \lambda & \lambda & \lambda+2G & 0 & 0 & 0 \\ 0 & 0 & 0 & G & 0 & 0 \\ 0 & 0 & 0 & 0 & G & 0 \\ 0 & 0 & 0 & 0 & 0 & G \end{bmatrix} \tag{11}$$

where G is the shear modulus and λ is the Lamé's parameter. These parameters are related to the elastic modulus E and Poisson ratio ν by the following relation:

$$G = \frac{E}{2(1+\nu)} \quad \lambda = \frac{\nu E}{(1+\nu)(1-2\nu)} \tag{12}$$

4.2 Fundamental nuclei

The generalised displacement vector $\mathbf{u}_\tau$ is interpolated along the y direction by means of the shape functions N_i, according to FEM classical procedure:

$$\boldsymbol{u}(x,y,z) = F_\tau(x,z)N_i(y)\boldsymbol{u}_{\tau i} \tag{13}$$

where $\mathbf{u}_{\tau i}$ is the nodal unknown vector. For the sake of brevity, the properties of the shape functions are not reported in the present paper. More details on FEM can be found, for example, in [39]. In the present work four-node (B4) 1D elements which lead to a cubic approximation along the y axis have been used. Given the principle of virtual displacements, the internal strain energy L_{int} can be related to the work of the inertial loads L_{ine} as follows:

$$\delta L_{\text{int}} = \int_V \delta\boldsymbol{\epsilon}^T \boldsymbol{\sigma}\, dV = -\delta L_{\text{ine}} \tag{14}$$

Where δ stands for virtual variation. Considering Eqs. 8, 10 and 13, the virtual variation of the strain energy can be written in a compact form:

$$\delta L_{\text{int}} = \delta\boldsymbol{u}_{\tau i}^T \mathbf{K}^{ij\tau s}\boldsymbol{u}_{sj} \tag{15}$$

where $\mathbf{K}^{ij\tau s}$ is the fundamental nucleus of the stiffness matrix and the superscripts indicate the four indexes exploited to expand the elemental matrix: τ and s are related to the expansion functions F_τ and F_s whereas i and j are related to the shape functions N_i and N_j. The fundamental nucleus, which is a 3x3 array, is formally independent of the order of the beam model. A more detailed explanation of the expansion of nuclei and assembly procedures in FEM framework can be found in [39].

The work of the inertial loadings can be written in terms of virtual variation:

$$\delta L_{\text{ine}} = \int_V \rho \ddot{\mathbf{u}} \delta \mathbf{u}^T \, dV \tag{16}$$

In the above equation ρ stands for the density of the material, whereas $\ddot{\mathbf{u}}$ is the acceleration vector. By substituting Eq. 13 into Eq. 16, one has

$$\delta L_{\text{ine}} = -\delta \boldsymbol{u}_{\tau i}^T \int_L N_i N_j \, dy \int_\Omega \rho F_\tau F_s \, d\Omega \ddot{\mathbf{u}}_{sj} = -\delta \boldsymbol{u}_{\tau i}^T \mathbf{M}^{ij\tau s} \ddot{\mathbf{u}}_{sj} \tag{17}$$

where $\ddot{\mathbf{u}}_{sj}$ indicates the nodal acceleration vector and $\mathbf{M}^{ij\tau s}$ is the fundamental nucleus of the elemental mass matrix, whose components are:

$$\begin{gathered} \mathbf{M}_{xx}^{ij\tau s} = \mathbf{M}_{yy}^{ij\tau s} = \mathbf{M}_{zz}^{ij\tau s} = \int_L N_i N_j \, dy \int_\Omega \rho F_\tau F_s \, d\Omega \\ \mathbf{M}_{xy}^{ij\tau s} = \mathbf{M}_{xz}^{ij\tau s} = \mathbf{M}_{yx}^{ij\tau s} = \mathbf{M}_{zx}^{ij\tau s} = \mathbf{M}_{yz}^{ij\tau s} = \mathbf{M}_{zy}^{ij\tau s} = 0 \end{gathered} \tag{18}$$

Even in the case of inertial terms, no assumptions have been made on the expansion order of the theory; thus, several refined beam models can be developed using this formulation without any formal change in the fundamental nucleus components.

The undamped dynamic problem is obtained by substituting the fundamental nuclei into the principle of virtual displacement (Eq. 14), by expanding the CUF fundamental indexes and by assembling the global FEM arrays.

$$\mathbf{M}\ddot{\mathbf{u}} + \mathbf{K}\mathbf{u} = 0 \tag{19}$$

In the present work, the boundary conditions are applied by using the penalization method, which is a classical procedure in FEM.

Considering harmonic solutions, the second-order system of ordinary differential equations in Eq. (19) results into a classical eigenvalue problem:

$$(-\omega_k^2 \mathbf{M} + \mathbf{K})\mathbf{u}_k = 0 \tag{20}$$

where $\mathbf{u}_k$ is the *k-th* eigenvector.

4.3 Mode Superposition Method

Given a system with multiple degrees of freedom (DOFs), the equilibrium governing equations of the dynamic response are [66]:

$$\boldsymbol{M}\ddot{\boldsymbol{u}}(t) + \boldsymbol{C}\dot{\boldsymbol{u}}(t) + \boldsymbol{K}\boldsymbol{u}(t) = \boldsymbol{P}(t) \tag{21}$$

where $\boldsymbol{C}$ is the damping matrix and $\boldsymbol{P}$ is the time-dependant loading vector, which is computed in the framework of CUF as in [39]. According to the superposition method, the unknowns vector $\boldsymbol{u}$ is transformed as follows:

$$\boldsymbol{u}(t) = \boldsymbol{\Phi}\boldsymbol{x}(t) \tag{22}$$

where $\boldsymbol{\Phi}$ is a $DOFs \times m$ matrix containing m $\boldsymbol{M}$-orthonormalized eigenvectors and $\boldsymbol{x}(t)$ is a time-dependent vector of order m. Hence, the equations of motion can be transformed by substituting Eq. 22 into the governing equations (Eq. 21) and pre-multiplying each term by $\boldsymbol{\Phi}^T$

$$\ddot{\boldsymbol{x}}(t) + \boldsymbol{\Phi}^T\boldsymbol{C}\boldsymbol{\Phi}\dot{\boldsymbol{x}}(t) + \boldsymbol{\Omega}^2\boldsymbol{x}(t) = \boldsymbol{\Phi}^T\boldsymbol{P}(t) \tag{23}$$

where $\boldsymbol{\Omega}^2$ is the diagonal matrix that stores the eigenvalues ω_i^2. It can be noticed from Eq. 23 that the equations of motion are decoupled if the damping is neglected. The resulting relation can be decomposed in m individual equations whose solution can be obtained by means of the Duhamel integral

$$\left.\begin{aligned} \ddot{x}_i(t) + \omega_i^2 x_i(t) &= r_i(t) \\ r_i(t) &= \boldsymbol{\Phi}_i\boldsymbol{P}(t) \end{aligned}\right\} \qquad i = 1, 2, ..., n \tag{24}$$

$$x_i(t) = \frac{1}{\omega_i}\int_0^t r_i(\tau)\sin\omega_i(t-\tau)d\tau + \alpha_i\sin\omega_i t + \beta_i\cos\omega_i t \tag{25}$$

Initial conditions are needed to compute α_i and β_i .

Once the solution for each of the m equations is calculated, the contribution to the response for each mode is obtained.

$$\boldsymbol{u}^m(t) = \sum_{i=1}^{m}\boldsymbol{\Phi}_i x_i(t) \tag{26}$$

Of course, the accuracy of the solution will depend on m. Equation 24 can be decoupled even in the simple case of proportional damping:

$$\boldsymbol{\Phi}_i^T\boldsymbol{C}\boldsymbol{\Phi}_j = 2\omega_i\xi_i\delta_{ij} \tag{27}$$

where ξ_i is a modal damping parameter and δ_{ij} is the Kronecker delta ($\delta_{ij} = 1$ for $i = j$, $\delta_{ij} = 0$ otherwise). In this case, in fact, the eigenvectors are also $\boldsymbol{C}$-orthonormal and the response can be obtained by means of the Duhamel integral

$$x_i(t) = \frac{1}{\overline{\omega}_i}\int_0^t r_i(\tau)e^{-\xi_i\omega_i(t-\tau)}\sin\overline{\omega}_i(t-\tau)d\tau + e^{-\xi_i\omega_i t}\left(\alpha_i\sin\overline{\omega}_i t + \beta_i\cos\overline{\omega}_i t\right) \tag{28}$$

where $\overline{\omega}_i = \omega_i\sqrt{1-\xi_i^2}$ and α_i and β_i are calculated from the initial conditions.

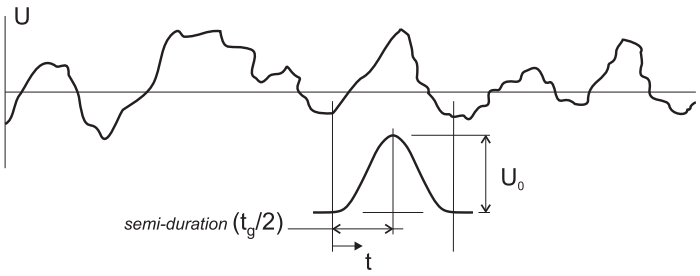

Figure 2: One-minus-cosine discrete gust idealization

In this work the Rayleigh damping is considered

$$\boldsymbol{C} = \alpha \boldsymbol{M} + \beta \boldsymbol{K} \tag{29}$$

since α and β are constants, the model adopted is a proportional damping. Further information about dynamic response analysis and related solution methodologies can be found in [1, 57, 66].

5 Time-varying Inertial Loads

In this paper, considerable attention is focused on the response to inertial loads. Inertial loads have been introduced in the framework of CUF in [67]. In general, the equivalent load vector due to an applied acceleration field, $\ddot{\boldsymbol{u}}_0$, is calculated by evaluating the virtual variation of the work of the external loadings as follows:

$$\delta L_{\text{ext}} = \int_V \rho \delta \boldsymbol{u}^T \ddot{\boldsymbol{u}}_0 \, dV \tag{30}$$

Typical inertial loads are gust loads. Gust loads are generally considered as the result of a change in angle of attack due to a component of the gust velocity (U). In case of a vertical gust, the change of angle of attack ($\Delta\alpha$), in radians, is assumed approximately equal to the gust velocity divided by the aircraft speed (V_∞). The lift change caused by the gust and the incremental load factor Δn can be defined as

$$\Delta L = \tfrac{\rho_\infty}{2} V_\infty^2 S C_{L_\alpha} \Delta\alpha \qquad \Delta n = \tfrac{\Delta L}{W} = \frac{\frac{\rho_\infty}{2} U V_\infty}{\left(\frac{W}{C_{L_\alpha} S}\right)} \tag{31}$$

where ρ_∞ indicates the air density and $\frac{\rho_\infty}{2} V_\infty^2$ is the dynamic pressure; S and C_{L_α} are the reference wing area and the lift curve slope, respectively.

In this paper, a temporally distributed discrete gust idealization is adopted. The gust structure can be modeled as the one-minus-cosine pulsed function shown in Fig. 2. As reported in [56], the gust is defined as

follows

$$U(t) = \frac{1}{2}U_0\left(1 - cos\frac{2\pi t}{t_g}\right) \tag{32}$$

where t_g is the duration of the gust and U_0 is the design gust velocity. The time-dependant incremental load factor can be computed by substituting Eq. (32) into Eq. (31),

$$\Delta n = \frac{\frac{\rho_\infty}{2}U_0 V_\infty}{\left(\frac{W}{C_{L_\alpha}S}\right)}\left(1 - cos\frac{2\pi t}{t_g}\right) \tag{33}$$

For a more detailed dissertation about discrete gust idealization, the reader is referred to [55, 56, 57]. This paper investigates the dynamic response of straight wings subjected to discrete gust loads. These loads cause the deformation of the structure, modifying the aerodynamic forces acting on the wing. In general, this aspect requires the modification of the value of C_{L_α} used in Eq. 33. However, this aeroelastic phenomenon decreases as the sweep angle of the wing becomes small [55], so the reduction of C_{L_α} has been neglected in the present paper. Moreover, all the aspects related to the unsteadiness of the aerodynamics, which plays a fundamental role in gust response as detailed in [56] and [68], are not considered in the present preliminary study.

6 Numerical Results

This section presents results concerning the dynamic response of one-dimensional CUF models by means of the modal superposition method. A preliminary assessment to validate the accuracy of CUF based finite elements is performed, whereas the second part focuses on the dynamic response analysis of typical aerospace structures, such as wing-box and complete wing structures.

6.1 Compact square section

A simply supported square-section beam is considered. The sides have 0.1 m dimension, the span-to-height ratio L/h is 100 and the material properties are: $E = 69$ GPa, $\nu = 0.33$ and $\rho = 2700\ \frac{kg}{m^3}$. The structure is modeled by means of 10 B4 beam elements along the y axis, and it is loaded with a single harmonic load applied at the center of the mid-span section of the beam:

$$P_z(t) = P_{z0} sin(\omega t)$$

where $P_{z0} = -1000N$ is the amplitude of the sinusoidal load whereas $\omega = 7\frac{rad}{s}$ is the angular frequency. Let $\omega_1 > \omega$ be the fundamental angular frequency related to the first bending mode. Under the Euler-Bernoulli beam assumptions, the peak response by whether considering inertial term or not as well as the dynamic load factor can be written as follows [66]:

Theory	$u_{z_{max}DYN}$	$u_{z_{max}ST}$	ω_1	$\frac{u_{z_{max}DYN}}{u_{z_{max}ST}}$	$\frac{1}{1-\frac{\omega}{\omega_1}}$
Analytical	-69.4719	-36.2319	14.4030	1.9174	1.9456
EBBT	-70.4503	-36.2319	14.4023	1.9444	1.9456
TE_3	-70.0014	-36.2429	14.4006	1.9318	1.9459
TE_7	-70.0039	-36.2429	14.4006	1.9325	1.9459

Table 1: Maximum dynamic and static displacement [mm] obtained by means of different theories. Square beam subjected to sinusoidal load.

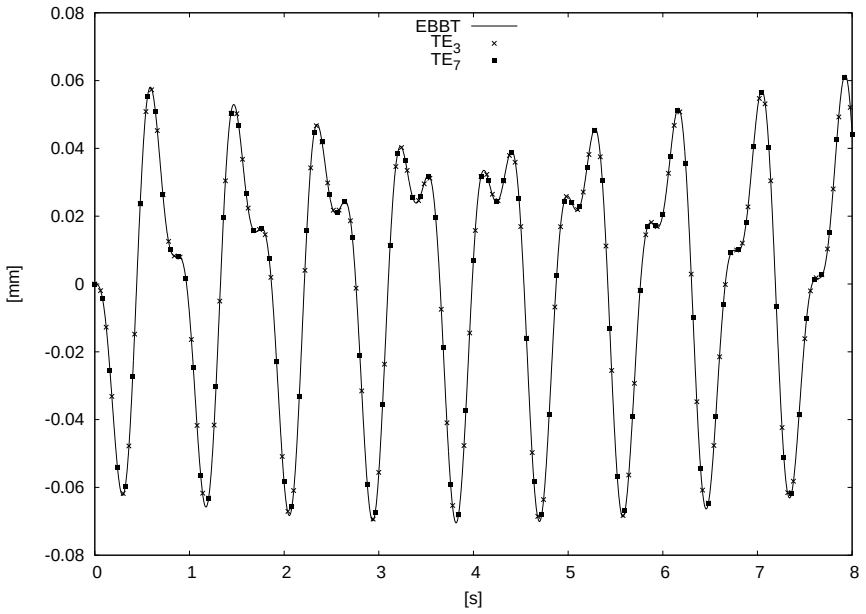

Figure 3: Transverse displacement at the mid-span section for various theories. Square beam under sinusoidal load.

$$u_{z_{max}DYN} \simeq \frac{2P_{z_0}L^3}{\pi^4 EI}\frac{1}{1-\frac{\omega}{\omega_1}} \quad u_{z_{max}ST} = \frac{2P_{z_0}L^3}{48EI} \simeq \frac{2P_{z_0}L^3}{\pi^4 EI}\frac{1}{1-\frac{\omega}{\omega_1}} \quad \frac{u_{z_{max}DYN}}{u_{z_{max}ST}} \simeq \frac{1}{1-\frac{\omega}{\omega_1}}$$

where $u_{z_{max}ST}$ is the displacement computed with Euler-Bernoulli model in the static case , $u_{z_{max}DYN}$ is the analytical undamped dynamic response of an Euler-Bernoulli beam, $\frac{u_{z_{max}DYN}}{u_{z_{max}ST}}$ is the Dynamic Load Factor (DLF), and I is the moment of inertia of the beam cross-section. The dynamic response is investigated by means of the modal superposition and the present CUF models over the time interval [0, 8] s . The results are reported in Table 1 in terms of maximum displacement in static and dynamic analysis for several expansion orders, whereas the trend as function of the time is shown in Fig. 3. The considered case shows good accordance between the results obtained by means of classical theories and those obtained using higher-order expansions. It is clear that slender beams with solid-section are well described by EBBT in cases which involve only bending phenomena.

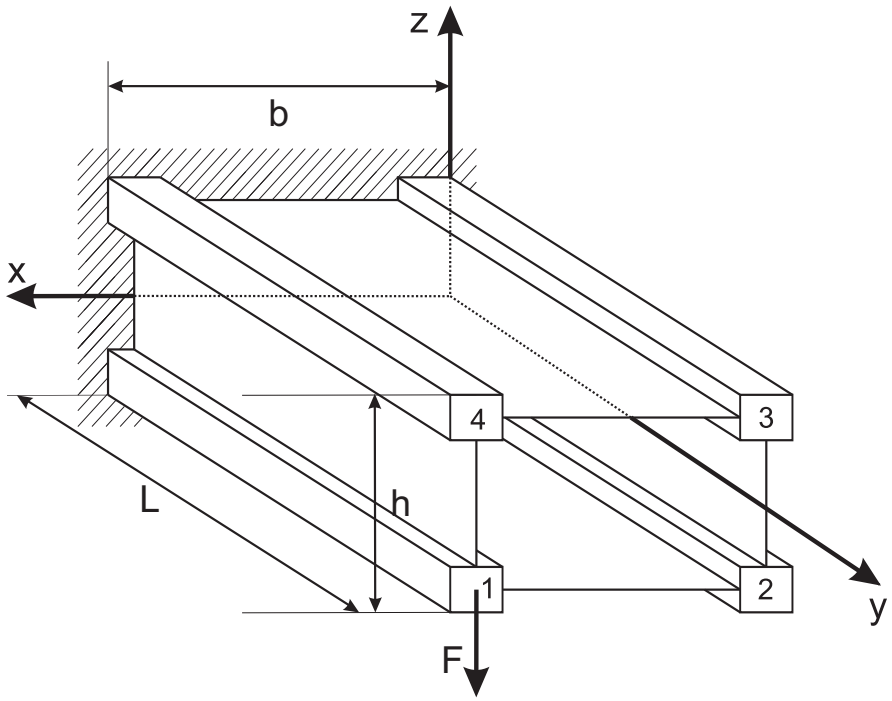

Figure 4: Application point of the sinusoidal load, wing-box model.

6.2 Wingbox

The dynamic response of a cantilever wing-box is investigated. The model consists of a rectangular reinforced structure whose dimensions are $L = 3$ m, $b = 1$ m and $h = 0.5$ m. The thickness of the panels is $t = 2 \times 10^{-3}$ m, the spar caps area is $A_s = 1.6 \times 10^{-3}\ m^2$, whereas the whole structure is made of aluminum alloy having the following properties: $E = 75$ GPa $\nu = 0.33$ and $\rho = 2770\ \frac{kg}{m^3}$. Analyses are also performed on a modification of the box by adding a transversal stiffener having thickness $r = t$ at the free edge. Static and free vibration analyses of these models have been performed in [49, 51]. Two different loading cases are considered in the present study, using TE, LE and CE theories. The first study involves a sinusoidal load having amplitude $F_0 = 10000N$ and angular frequency $\omega = 3\frac{rad}{s}$ whose application point is shown in Fig. 4. Time dependent transverse displacements at the load application point are reported in Fig. 5 for various theories. The maximum and minimum displacement at the center of each stringer is reported in Table 2 for the wing-box without rib and in Table 3 for the model with rib. Moreover, in the case of the wing-box without rib, the deformation of the tip cross-section, evaluated at $t = 0.5$ s and $t = 1.55$ s is reported in Fig. 6.

The results highlight the limits of classical theories. In fact, the wing-box without transversal stiffener undergoes a significant deformation of the cross-section, as shown in in Fig. 6. These warping effects can be observed also from the comparison between the displacements of each stringer reported in Table 2. Fig. 5 allows to observe the difference between the two configurations considered: it is clear that the addition of a rib increases the stiffness of the structure, which is subjected to lower deformations. Moreover, the presence of the stiffener decreases the differences between the results obtained by means of classical theories and those obtained using higher-order models. In fact, Table 3 shows a good accordance between classical and higher-

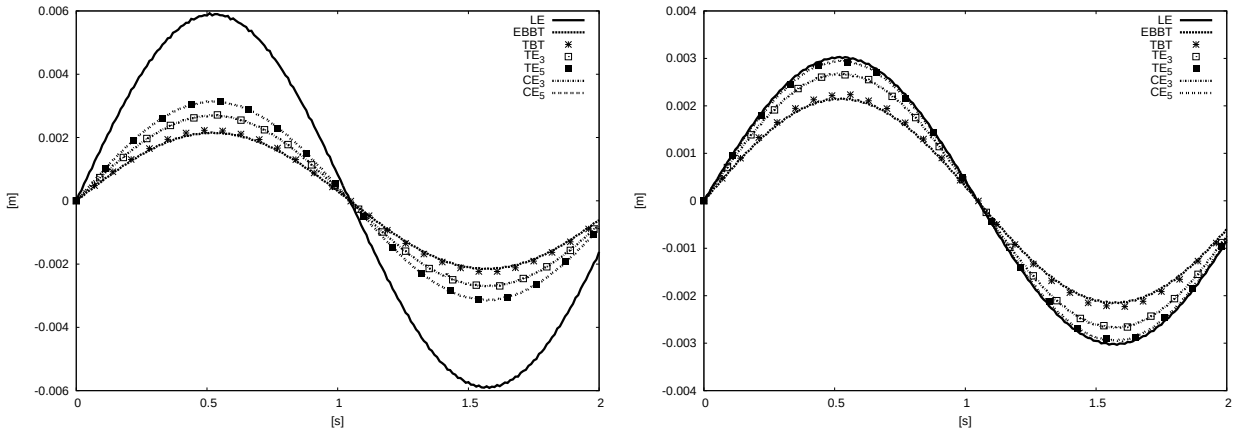

(a) Wingbox (b) Wingbox with Rib

Figure 5: Time dependent transverse displacement for various theories, wing-box model, sinusoidal loading case.

Theory	Stringer 1		Stringer 2		Stringer 3		Stringer 4	
	$u_{z_{max}}$	$u_{z_{min}}$	$u_{z_{max}}$	$u_{z_{min}}$	$u_{z_{max}}$	$u_{z_{min}}$	$u_{z_{max}}$	$u_{z_{min}}$
EBBT	2.1609	−2.1577	2.1609	−2.1577	2.1609	−2.1577	2.1609	−2.1577
TBT	2.2437	−2.2475	2.2437	−2.2475	2.2437	−2.2475	2.2437	−2.2475
TE_3	2.7147	−2.7136	2.3594	−2.3572	2.3589	−2.3567	2.7141	−2.7130
TE_5	3.1402	−3.1457	2.0593	−2.0612	2.0575	−2.0594	3.1384	−3.1440
CE_3	2.7064	−2.7052	2.3567	−2.3544	2.3565	−2.3542	2.7061	−2.7050
CE_5	3.1403	−3.1459	2.0593	−2.0613	2.0575	−2.0595	3.1385	−3.1441
LE	5.9281	−5.9129	0.6764	−0.6783	0.6764	−0.6783	5.9281	−5.9129

Table 2: Maximum and minimum transverse displacement [mm] at the tip obtained by means of different theories. Wing-box, sinusoidal load.

Theory	Stringer 1		Stringer 2		Stringer 3		Stringer 4	
	$u_{z_{max}}$	$u_{z_{min}}$	$u_{z_{max}}$	$u_{z_{min}}$	$u_{z_{max}}$	$u_{z_{min}}$	$u_{z_{max}}$	$u_{z_{min}}$
EBBT	2.1620	−2.1593	2.1620	−2.1593	2.1620	−2.1593	2.1620	−2.1593
TBT	2.2512	−2.2479	2.2512	−2.2479	2.2512	−2.2479	2.2512	−2.2479
TE_3	2.6873	−2.6876	2.3973	−2.3974	2.3971	−2.3972	2.6871	−2.6874
TE_5	2.9533	−2.9497	2.2538	−2.2510	2.2511	−2.2482	2.9503	−2.9467
CE_3	2.6873	−2.6876	2.3974	−2.3974	2.3972	−2.3972	2.6871	−2.6874
CE_5	2.9580	−2.9543	2.2387	−2.2363	2.2385	−2.2361	2.9577	−2.9541
LE	3.0304	−3.0345	2.2721	−2.2773	2.2721	−2.2773	3.0304	−3.0345

Table 3: Maximum and minimum transverse displacement [mm] at the tip obtained by means of different theories. Wing-box with rib, sinusoidal load.

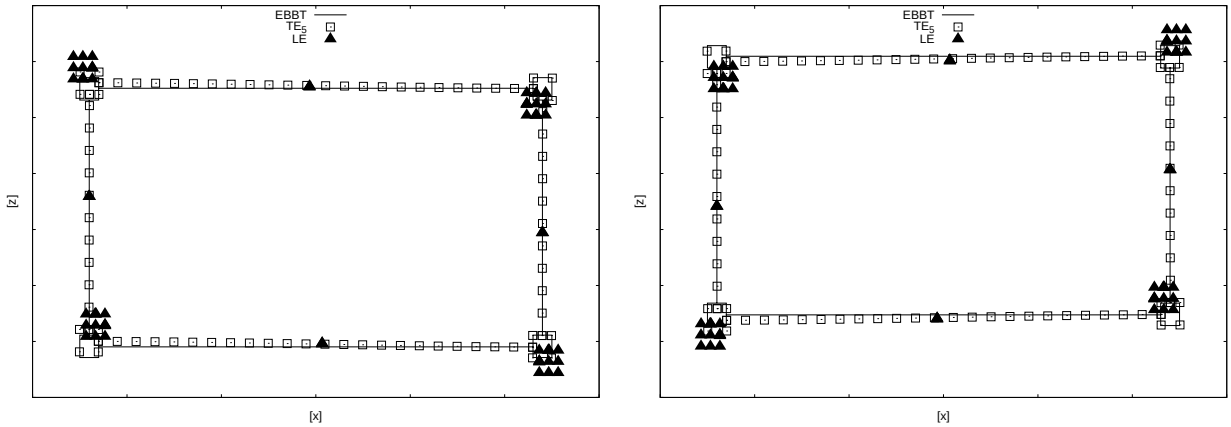

(a) t = 0.5 s (b) t = 1.55 s

Figure 6: Deformation of the tip cross-section of the wing-box with no rib, sinusoidal loading case.

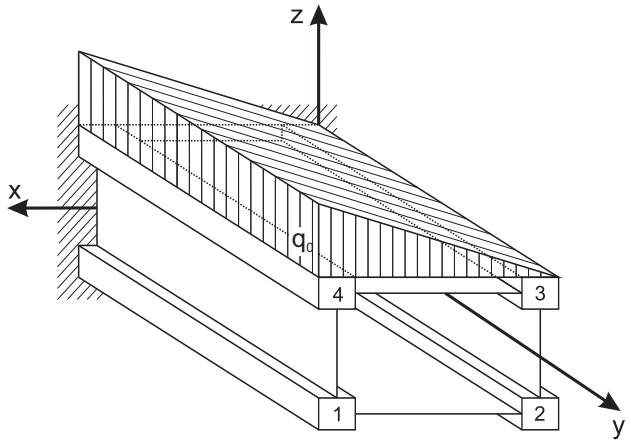

Figure 7: Load distribution on the cross-section.

order theories for this case.

In the second analysis case, the wing-box subjected to a pressure load whose distribution across the section is shown in Fig. 7. The load, uniformly distributed in the span-wise direction, is modeled as a function of time according to the following relation:

$$q = \begin{cases} \frac{q_0}{t_1} \cdot t, & t \in [0, t_1] \\ q_0, & t > t_1 \end{cases} \tag{34}$$

The analysis is performed considering $t_1 = 0.05$ s and $q_0 = \frac{10000}{3} \frac{N}{m}$. The maximum displacement at the center of the stringers and the horizontal panels is reported in Table 4 and Table 5 for the two configurations of the structure. In the case of wing-box without rib, the transverse displacement obtained by means of different theories is shown in Fig.8(a) for the component evaluated at the center of the stringer 1, whereas Fig.8(b) shows the values obtained at the center of the upper panel. Moreover, the deformation of the tip cross-section evaluated at $t = 0.57$ s is reported in Fig. 9 for EBBT, higher-order Taylor and Lagrange models.

It is clear, for this loading case, that classical theories provide unreliable results. As shown in Fig. 9, the

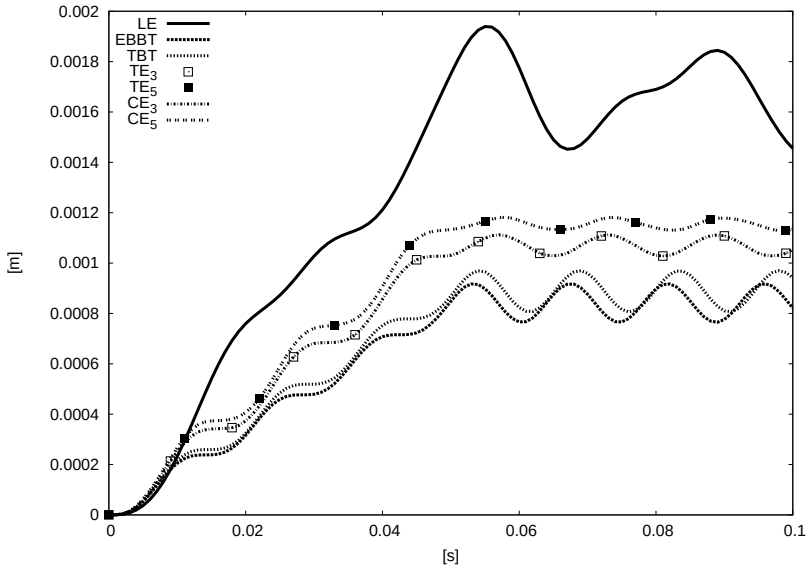

(a) Wingbox: stringer 1 at y = L

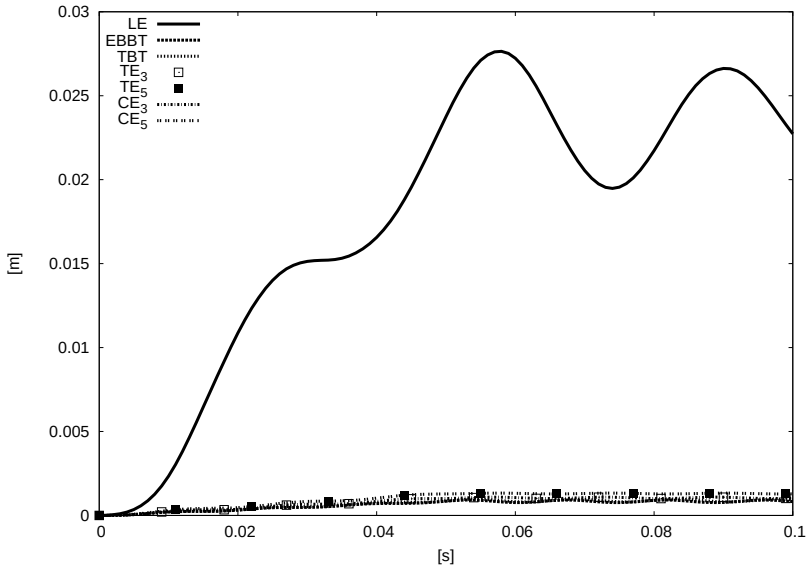

(b) Wingbox: upper panel at y = L

Figure 8: Time dependent transverse displacement for various theories, wing-box model, linear loading case.

Theory	Stringer 1	Stringer 2	Stringer 3	Stringer 4	Upper Panel	Lower Panel
EBBT	0.9178	0.9178	0.9178	0.9178	0.9178	0.9178
TBT	0.9697	0.9697	0.9697	0.9697	0.9697	0.9697
TE_3	1.1123	1.0632	1.0634	1.1124	1.0888	1.0880
TE_5	1.1807	1.0315	1.0349	1.1841	1.3299	0.8967
CE_3	1.1124	1.0631	1.0632	1.1125	1.0886	1.0880
CE_5	1.1818	1.0330	1.0362	1.1851	1.3295	0.8939
LE	1.9392	0.8300	0.8318	1.9423	27.6448	−5.5371

Table 4: Maximum transverse displacement [mm] at the tip obtained by means of different theories. Wingbox, linear load.

Theory	Stringer 1	Stringer 2	Stringer 3 (Tip)	Stringer 4	Upper Panel	Upper Panel (Mid-span)
EBBT	0.9151	0.9151	0.9151	0.9151	0.9151	0.3573
TBT	0.9546	0.9546	0.9546	0.9546	0.9546	0.3917
TE_3	1.0685	1.0231	1.0230	1.0684	1.0465	0.4945
TE_5	1.1639	1.0488	1.0402	1.1556	1.1070	0.6278
CE_3	1.0676	1.0222	1.0221	1.0675	1.0457	0.4938
CE_5	1.1592	1.0445	1.0419	1.1568	1.1040	0.5495
LE	1.4093	1.2717	1.2537	1.3796	1.3579	7.9432

Table 5: Maximum transverse displacement [mm] obtained by means of different theories. Wingbox with rib, linear load.

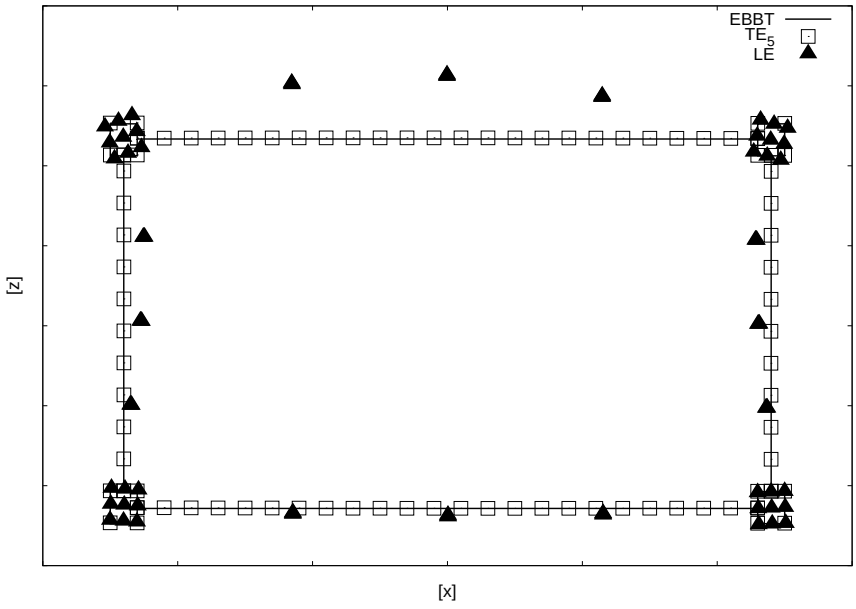

Figure 9: Deformation of the cross-section at t = 0.57 s, linear loading case.

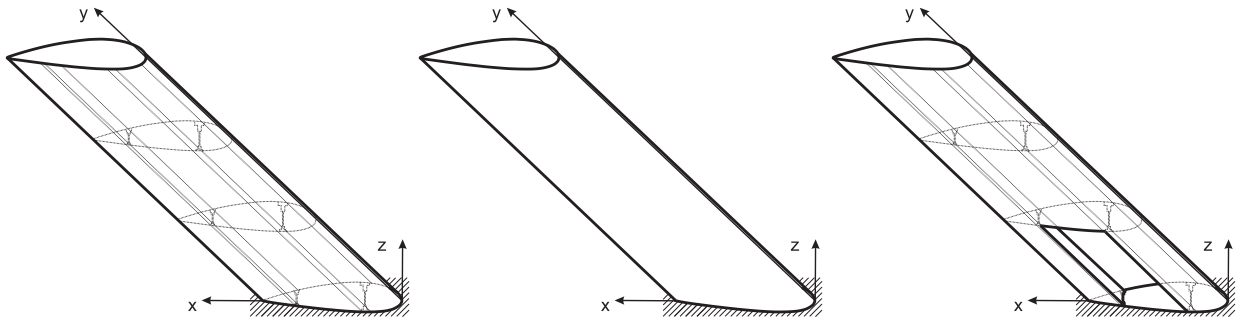

(a) Configuration A : Complete Wing (b) Configuration B : Skin Only (c) Configuration C : Open Bay

Figure 10: Wing configurations.

EBBT model is not able to detect the deformation of the cross-section caused by the distributed load applied on the upper surface. On the other hand, the LE model is capable to describe the warping phenomena which involve the panels and the effects concerning the stringers, which are subjected to torsion. Moreover, from the comparison between the displacements evaluated for various theories reported in Table 4, it is clear that these values are underestimated by classical and lower order theories. These limits can be observed also from the time history shown in Fig. 8(a) and Fig. 8(b). Also in this case, the addition of the transversal stiffener slightly reduces the difference of the results evaluated at the tip, as reported in Table 5. However, the limits of lower order theories are blatantly evident if the displacement of the upper panel at the mid span (column 7) is considered.

6.3 Aircraft wing

The structure considered in this section consists in an aircraft wing in various configurations. A NACA 2415 airfoil cross-section was used, with 6 m length and 1 m chord, as shown in Fig. 10(a). Clamped-free boundary conditions are addressed, whereas the material is the same used in the previous case. The whole structure is discretized by means of CUF L9 elements, as reported in [51]. In order to investigate the behaviour of a thin-walled structure, the model is modified as shown in Fig. 10(b). In this case, the contribution of the transversal stiffeners and the longerons is neglected. Moreover, the effect of the presence of an open bay is evaluated, considering the model shown in Fig. 10(c). In the first case, a single harmonic load having amplitude $F_0 = 1000$ N and angular frequency $\omega = 3$ rad/s is applied in $y = 1.996$ m as shown in Fig. 11. The transverse displacement evaluated using TE and LE theories at the trailing edge and the leading edge for the considered time interval is reported in Table 6, whereas time-dependent displacement of the leading edge and the trailing edge of the configurations A and C are shown in Fig. 12.

The data for configuration A in Fig. 12(a) show, in general, good accordance between the classical and LE theories considered. However, the results reported in Table 6 highlight that the torsional effects must be taken into account for a correct prediction of the behaviour of the structure. Moreover, from Fig. 12(b) it is possible to observe that the EBBT model leads to incorrect results if the model involves open sections or

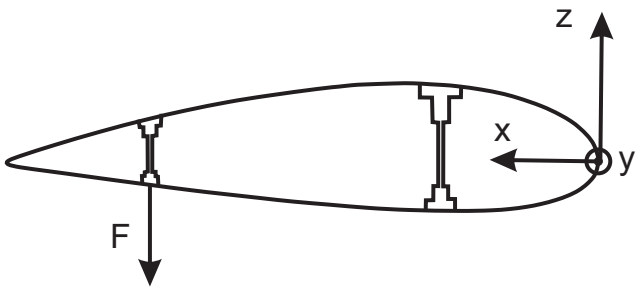

Figure 11: Application point of the harmonic force on the cross-section.

Point		EBBT	TBT	LE
Configuration A				
DOFs		84	140	24864
Leading Edge	$u_{z_{max}}$	6.036	6.045	5.711
	$u_{z_{min}}$	−6.183	−6.198	−5.866
Trailing Edge	$u_{z_{max}}$	6.036	6.045	6.102
	$u_{z_{min}}$	−6.183	−6.198	−6.261
Configuration B				
DOFs		84	140	14616
Leading Edge	$u_{z_{max}}$	8.591	8.593	8.211
	$u_{z_{min}}$	−8.696	−8.711	−8.277
Trailing Edge	$u_{z_{max}}$	8.591	8.593	9.213
	$u_{z_{min}}$	−8.696	−8.711	−9.299
Configuration C				
DOFs		84	140	24450
Leading Edge	$u_{z_{max}}$	8.319	8.318	7.690
	$u_{z_{min}}$	−7.879	−7.889	−7.253
Trailing Edge	$u_{z_{max}}$	8.319	8.318	9.084
	$u_{z_{min}}$	−7.879	−7.889	−8.594

Table 6: Maximum and minimum u_z displacement [mm] at the tip of the wing obtained by means of different theories, various configurations of the wing subjected to sinusoidal load.

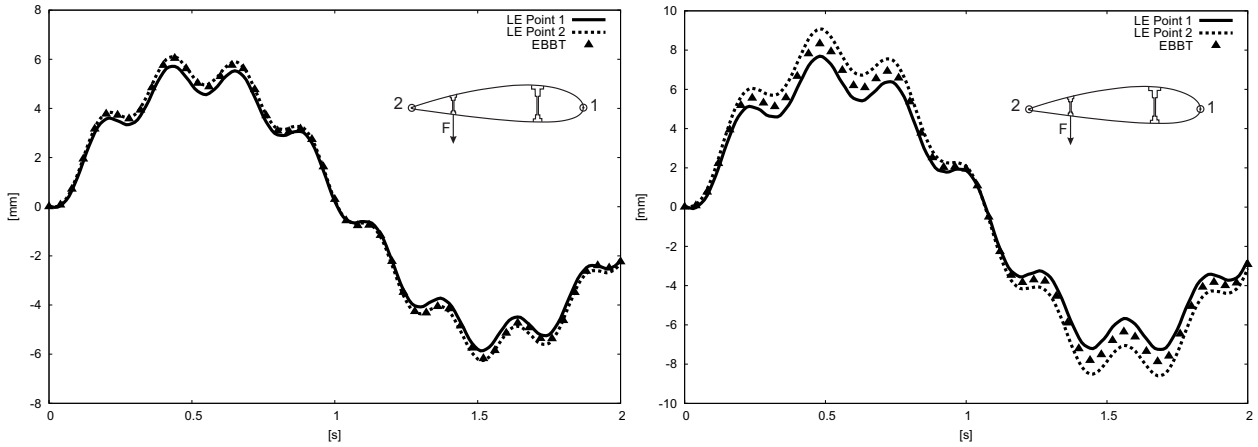

(a) Configuration A

(b) Configuration C

Figure 12: Time-dependent transverse displacement at the tip for various theories. Configurations A and C of the wing subjected to sinusoidal load.

Point		EBBT	TBT	LE
Configuration A				
DOFs		84	140	24864
Leading Edge	$u_{z_{max}}$	67.192	67.256	66.878
	$u_{z_{min}}$	−23.539	−23.627	−22.914
Trailing Edge	$u_{z_{max}}$	67.192	67.256	67.705
	$u_{z_{min}}$	−23.539	−23.627	−23.177
Configuration B				
DOFs		84	140	14616
Leading Edge	$u_{z_{max}}$	58.202	58.254	59.298
	$u_{z_{min}}$	−13.934	−14.001	−16.711
Trailing Edge	$u_{z_{max}}$	58.202	58.254	61.429
	$u_{z_{min}}$	−13.934	−14.001	−17.391
Configuration C				
DOFs		84	140	24450
Leading Edge	$u_{z_{max}}$	88.425	88.406	89.484
	$u_{z_{min}}$	−48.484	−48.481	−49.190
Trailing Edge	$u_{z_{max}}$	88.425	88.406	91.570
	$u_{z_{min}}$	−48.484	−48.481	−50.202

Table 7: Maximum and minimum u_z displacement [mm] at the tip obtained by means of different theories, various configurations of the wing subjected to gust loads.

stiffness members are not modeled. This is also clear from Table 6. Since torsional and local effects are not taken into account, classical and lower order theories provide poor results for these cases.

6.3.1 Gust pulse analysis

The effect of a gust load is then investigated. Considering a wing loading $\frac{W}{S} = 378.6\ \frac{kg}{m^2}$, the following flight conditions at sea level are addressed: $\rho_\infty = 1.225\ \frac{kg}{m^3}$, $V_\infty = 80$ m/s. A vertical gust having intensity $U_0 = 10$ m/s and duration $t_g = 0.4$ s is encountered at 1-g flight conditions. Assuming inviscid flow, a $C_{L_\alpha} = 7.6\ rad^{-1}$ was estimated by means of XFLR5 [69] and XFoil [70] softwares. The transverse displacement evaluated at the leading edge and the trailing edge is reported in Table 7 for the three proposed wing structures. Moreover, the effect of the parameter t_g is investigated. In fact, Fig. 13(a), Fig. 13(b) and Fig. 13(c) report the time dependent displacement of the trailing edge for the configurations A, B and C, respectively.

Since the gust load primary involves the bending of the structure, in the case of the reinforced structure considered in configuration A the classical theories provide results which are in good accordance with those obtained using the LE model. This is evident from the observation of Fig. 13(a) and rows 4-7 of Table 7. On the other hand, the deviation of these models is clear in the case of thin-walled structures and open sections. In both cases a refined theory is needed to predict the behaviour of the structure with the desired degree of accuracy.

For the last analysis, the effect of the damping parameter is investigated. Figure 14 allows one to evaluate the effect of the β parameter reported in Eq. 29 on the dynamic behaviour of the structure. The analysis is performed considering $t_g = 0.4$ s and $\beta = 0.01$. It is clear, for the models proposed, that the introduction

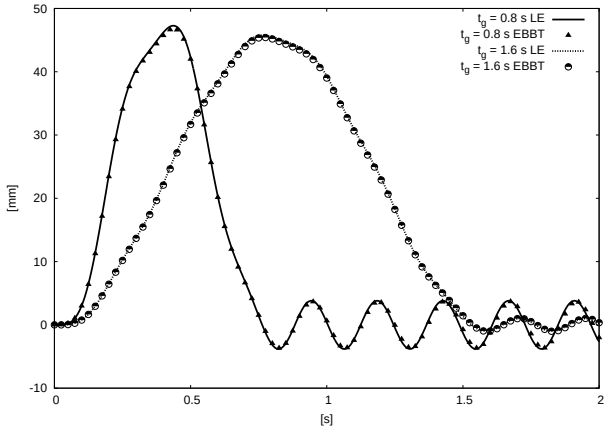

(a) Configuration A

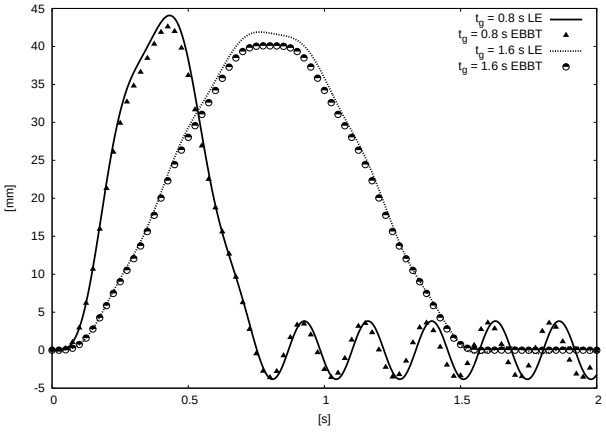

(b) Configuration B

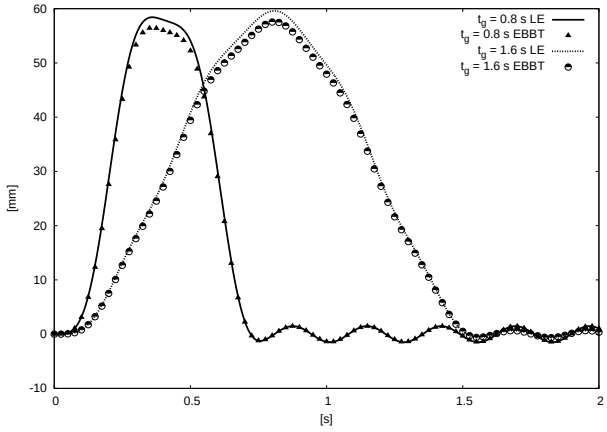

(c) Configuration C

Figure 13: Time-dependent transverse displacement at the trailing edge of the wing tip for $t_g = 0.8s$ and $t_g = 1.6s$, various configurations of the wing subjected to gust loads.

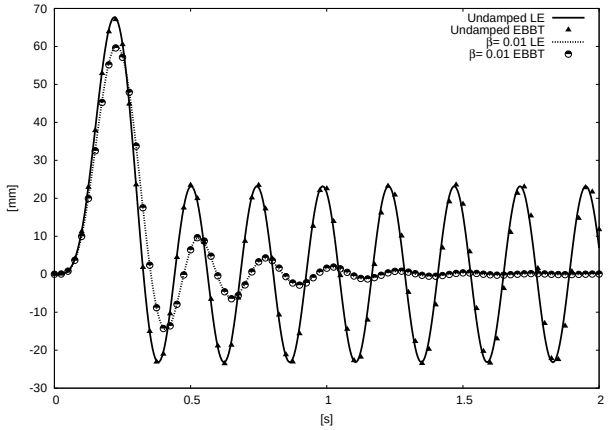

(a) Configuration A

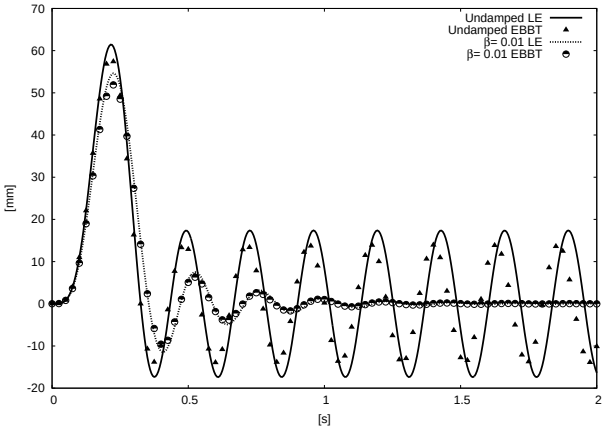

(b) Configuration B

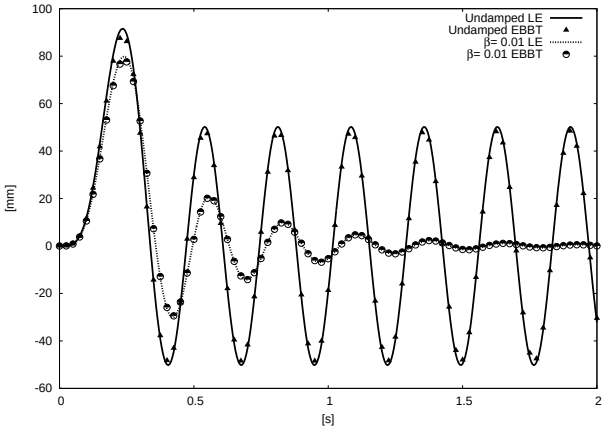

(c) Configuration C

Figure 14: Time-dependent transverse displacement at the trailing edge of the wing tip for $t_g = 0.4s$ in the case of the undamped and damped system, various configurations of the wing subjected to gust loads.

of this parameter leads to the damping of the oscillations which involve the structure. On the other hand, in the undamped system it is possible to observe that the oscillations maintain the same amplitude after the perturbation induced by the gust.

7 Conclusions

The dynamic response of typical aerospace structures, including thin-walled and open-section wing boxes, has been investigated in this paper. The analyses have been performed by employing the mode superposition method in conjunction with the Carrera Unified Formulation (CUF). It has been highlighted, for the loading cases considered, that:

- The models investigated undergo significant higher-order phenomena, such as, for example, bending/torsion couplings and local effects.
- 1D refined CUF provide us with a general formulation able to give accurate and efficient solutions. CUF beam models, and particularly CW, are, in fact, able to deal with bending/torsional couplings, differential bending, warping, and in-plane cross-sectional distortions. Those effects can only be described by 2D and 3D finite elements, or by ad-hoc higher-order models.
- Classical beam theories provide inaccurate results for most of the cases considered.
- Nonetheless, the introduction of transversal stiffeners reduces the difference between the results obtained using classical and refined theories.

In the present paper, various beam theories for the dynamic analysis of aircraft structures have been developed by employing the hierarchical capabilities of CUF. Namely, Taylor Expansion (TE), Chebyshev Expansion (CE) and Lagrange Expansion (LE) models have been formulated. The main advantages of CUF refined models are: (i) the formal structure of the FE arrays does not depend on the beam order and class; (ii) refined models can be automatically obtained by opportunely increasing the number of terms in the beam kinematics and choosing a suitable set of F_τ functions; the same accuracy of 2D and 3D FE models can be obtained with 1D CUF elements.

Particular attention has been focused on the Component-Wise (CW) approach deriving from the LE CUF formulation. The CW methodology allows one to model each part of a multi-component structure as a refined 1D beam element, thus avoiding the geometrical inconsistencies of classical approaches. The CW models have shown the accuracy and numerical efficiency of this formulation in the investigation of the dynamic response of aerospace structures. Moreover, thanks to its hierarchical characteristics, CUF models can be used in both preliminary and advanced design phases. In fact, the model accuracy can be easily improved, because it is a simple input of the analysis.

References

[1] K.J. Bathe. *Finite element procedure*. Prentice hall, Upper Saddle River, New Jersey, 1996.

[2] L. Euler. *De curvis elasticis*. Bousquet, Geneva, 1744.

[3] S.P. Timoshenko. On the corrections for shear of the differential equation for transverse vibration of prismatic bars. *Philosophical Magazine*, 41:744–746, 1922. doi: 10.1080/14786442108636264.

[4] S.P. Timoshenko. On the transverse vibrations of bars of uniform cross section. *Philosophical Magazine*, 41:122–131, 1922. doi: 10.1080/14786442208633855.

[5] S.P. Timoshenko and J.N. Goodier. *Theory of elasticity*. McGraw-Hill, New York, 1970.

[6] F. Gruttmann, R. Sauer, and W. Wagner. Shear stresses in prismatic beams with arbitrary cross-sections. *International Journal for Numerical Methods in Engineering*, 45:865–889, 1999.

[7] W. Wagner and F. Gruttmann. A displacement method for the analysis of flexural shear stresses in thin walled isotropic composite beams. *Computers and Structures*, 80:1843–1851, 2002. doi: 10.1016/S0045-7949(02)00223-7.

[8] F. Gruttmann and W. Wagner. Shear correction factors in Timoshenko's beam theory for arbitrary shaped cross-sections. *Computational Mechanics*, 27:199–207, 2001. doi: 10.1007/s004660100239.

[9] N.G. Stephen and M. Levinson. A second order beam theory. *Journal of Sound and Vibration*, 67(3):293–305, 1979. doi : 10.1016/0022-460X(79)90537-6.

[10] M. Levinson. A new rectangular beam theory. *Journal of Sound and Vibration*, 74(1):81–87, 1981. doi : 10.1016/0022-460X(81)90493-4.

[11] Z. Rychter. On the accuracy of a beam theory. *Mechanics Research Communications*, 14(2):99–105, 1987. doi : 10.1016/0093-6413(87)90024-3.

[12] R.K. Kapania and S. Raciti. Recent advances in analysis of laminated beams and plates, part ii: Vibrations and wave propagation. *AIAA Journal*, 27:935–946, 1989. doi : 10.2514/3.59909.

[13] P.R. Heyliger and J.N. Reddy. A higher order beam finite element for bending and vibration problems. *Journal of Sound and Vibration*, 126(2):309–326, 1988. doi : 10.1016/0022-460X(88)90244-1.

[14] T. Kant and A. Gupta. A finite element model for a higher-order shear-deformable beam theory. *Journal of Sound and Vibration*, 125(2):193–202, 1988. doi : 10.1016/0022-460X(88)90278-7.

[15] K.P. Soldatos and I. Elishakoff. A transverse shear and normal deformable orthotropic beam theory. *Journal of Sound and Vibration*, 155(3):528–533, 1992. doi : 10.1016/0022-460X(92)90717-C.

[16] S.R. Marur and T. Kant. Free vibration analysis of fiber reinforced composite beams using higher order theories and finite element modelling. *Journal of Sound and Vibration*, 194(3):337–351, 1996. doi : 10.1006/jsvi.1996.0362.

[17] S. R. Marur and T. Kant. On the angle ply higher order beam vibrations. *Computational Mechanics*, 40(1):25–33, 2007. doi : 10.1007/s00466-006-0079-0.

[18] T. Kant, S.R. Marur, and G.S. Rao. Analytical solution to the dynamic analysis of laminated beams using higher order refined theory. *Composite Structures*, 40(1):1–9, 1997.

[19] X. Tong, B. Tabarrok, and K.Y. Yeh. Vibration analysis of timoshenko beams with non-homogeneity and varying cross-section. *Journal of Sound and Vibration*, 186(5):821–835, 1995. doi : 10.1006/jsvi.1995.0490.

[20] L. Librescu and S. Na. Boundary control of free and forced oscillation of shearable thin-walled beam cantilevers. *European Journal of Mechanics, A/Solids*, 17(4):687–700, 1998.

[21] L. Ould Larbi, A. Kaci, M.S.A. Houari, and A. Tounsi. An efficient shear deformation beam theory based on neutral surface position for bending and free vibration of functionally graded beams. *Mechanics Based Design of Structures and Machines: An International Journal*, 41(4):421–433, 2013.

[22] P. Ladéveze, P. Sanchez, and J. Simmonds. Beamlike (Saint-Venant) solutions for fully anisotropic elastic tubes of arbitrary closed cross section. *Internatinal Journal of Solids & Structures*, 41(7):1925–1944, 2004. doi: 10.1016/j.ijsolstr.2003.11.006.

[23] P. Ladéveze and J. Simmonds. De nouveaux concepts en théorie des poutres pour des charges et des géométries quelconques. *Comptes Rendus Acad. Sci. Paris*, 332:445–462, 1996.

[24] P. Ladéveze and J. Simmonds. New concepts for linear beam theory with arbitrary geometry and loading. *European Journal Of Mechanics - A/Solids*, 17(3):377–402, 1998. doi: 10.1016/S0997-7538(98)80051-X.

[25] V. Berdichevsky, E. Armanios, and A. Badir. Theory of anisotropic thin-walled closed-cross-section beams. *Composites Engineering*, 2(5-7):411–432, 1992. doi: 10.1016/0961-9526(92)90035-5.

[26] V.V. Volovoi, D.H. Hodges, V.L. Berdichevsky, and V.G. Sutyrin. Asymptotic theory for static behavior of elastic anisotropic I-beams. *International Journal of Solid Structures*, 36(7):1017–1043, 1999. doi: 10.1016/S0020-7683(97)00341-7.

[27] V.V. Volovoi and D.H. Hodges. Theory of anisotropic thin-walled beams. *Journal of Applied Mechanics*, 67(3):453–459, 2000. doi: 10.1115/1.1312806.

[28] B. Popescu and D.H. Hodges. On asymptotically correct Timoshenko-like anisotropic beam theory. *International Journal of Solids and Structures*, 37:535–558, 2000. doi: 10.1016/j.ijsolstr.2003.11.006.

[29] W. Yu and D.H. Hodges. Generalized Timoshenko theory of the variational asymptotic beam sectional analysis. *Journal of the American Helicopter Society*, 50(1):46–55, 2005. doi: 10.4050/1.3092842.

[30] W. Yu and D.H. Hodges. Elasticity solutions versus asymptotic sectional analysis of homogeneous, isotropic, prismatic beams. *Journal of Applied Mechanics*, 71:15–23, 2004. doi: 10.1115/1.1640367.

[31] P. Subramanian. Dynamic analysis of laminated composite beams using higher order theories and finite elements. *Composite Structures*, 73(3):342–353, 2006. doi : 10.1016/j.compstruct.2005.02.002.

[32] R. Ganesan and A. Zabihollah. Vibration analysis of tapered composite beams using a higher-order finite element. part i: Formulation. *Composite Structures*, 77(3):306–318, 2007. doi : 10.1016/j.compstruct.2005.07.018.

[33] M. Şimşek and T. Kocatürk. Free vibration analysis of beams by using a third-order shear deformation theory. *Sadhana - Academy Proceedings in Engineering Sciences*, 32(3):167–179, 2007. doi : 10.1007/s12046-007-0015-9.

[34] E. Carrera, A. Pagani, M. Petrolo, and E. Zappino. Recent developments on refined theories for beams with applications. *Mechanical Engineering Reviews*, 2(2), 2015. ISSN 2187-9753.

[35] E. Carrera. Theories and finite elements for multilayered, anisotropic, composite plates and shells. *Archives of Computational Methods in Engineering*, 9(2):87–140, 2002. doi: 10.1007/BF02736649.

[36] E. Carrera. Theories and finite elements for multilayered plates and shells: a unified compact formulation with numerical assessment and benchmarking. *Archives of Computational Methods in Engineering*, 10(3):216–296, 2003. doi: 10.1007/BF02736224.

[37] E. Carrera, G. Giunta, and M. Petrolo. *Beam Structures Classical and Advanced Theories*. John Wiley & Sons, Ltd, The Atrium, Southern Gate, Chichester, West Sussex, PO19 8SQ, United Kingdom, 2011.

[38] E. Carrera and G. Giunta. Refined beam theories based on a unified formulation. *International Journal of Applied Mechanics*, 2(1):117–143, 2010. doi: 10.1142/S1758825110000500.

[39] E. Carrera, M. Cinefra, M. Petrolo, and E. Zappino. *Finite Element Analysis of Structures through Unified Formulation*. John Wiley & Sons Ltd, 2014.

[40] E. Carrera, G. Giunta, and M. Petrolo. *A Modern and Compact Way to Formulate Classical and Advanced Beam Theories*, chapter 4, pages 75–112. Saxe-Coburg Publications, Stirlingshire, UK, 2010. doi: 10.4203/csets.25.4.

[41] E. Carrera, M. Petrolo, and A. Varello. Advanced beam formulations for free vibration analysis of conventional and joined wings. *Journal of Aerospace Engineering*, 25(2), 2012. doi: 10.1061/(ASCE)AS.1943-5525.0000130.

[42] M. Petrolo, E. Zappino, and E. Carrera. Unified higher-order formulation for the free vibration analysis of one-dimensional structures with compact and bridge-like cross-sections. *Thin Walled Structures*, 56, 2012. doi: 10.1016/j.tws.2012.03.011.

[43] A. Pagani, M. Boscolo, J. R. Banerjee, and E. Carrera. Exact dynamic stiffness elements based on one-dimensional higher-order theories for free vibration analysis of solid and thin-walled structures. *Journal of Sound and Vibration*, 332(23):6104–6127, 2013. doi: 10.1016/j.jsv.2013.06.023.

[44] A. Pagani, E. Carrera, M. Boscolo, and J.R. Banerjee. Refined dynamic stiffness elements applied to free vibration analysis of generally laminated composite beams with arbitrary boundary conditions. *Composite Structures*, 110(0):305 – 316, 2014. doi : http://dx.doi.org/10.1016/j.compstruct.2013.12.010.

[45] S.M. Ibrahim, E. Carrera, M. Petrolo, and E. Zappino. Buckling of composite thin walled beams by refined theory. *Composite Structures*, 94(2):563–570, 2012. doi: 10.1016/j.compstruct.2011.08.020.

[46] E. Carrera and A. Varello. Dynamic response of thin-walled structures by variable kinematic one-dimensional models. *Journal of Sound and Vibration*, 331(24):5268–5282, 2012. doi: 10.1016/j.jsv.2012.07.006.

[47] E. Carrera and M. Petrolo. Refined beam elements with only displacement variables and plate/shell capabilities. *Meccanica*, 47(3):537–556, 2012.

[48] M. Filippi, A. Pagani, M. Petrolo, G. Colonna, and E. Carrera. Static and free vibration analysis of laminated beams by refined theory based on chebyshev polynomials. *Composite Structures*, 2015. Manuscript submitted for publication.

[49] E. Carrera, A. Pagani, and M. Petrolo. Classical, refined and component-wise analysis of reinforced-shell wing structures. *AIAA Journal*, 51(5):1255–1267, 2013. doi: 10.2514/1.J052331.

[50] E. Carrera, M. Maiaru, and M. Petrolo. Component-wise analysis of laminated anisotropic composites. *International Journal of Solids and Structures*, 49:1839–1851, 2012. doi: 10.1016/j.ijsolstr.2012.03.025.

[51] E. Carrera, A. Pagani, and M. Petrolo. Component-wise method applied to vibration of wing structures. *Journal of Applied Mechanics*, 80, 2013. doi: 10.1115/1.4007849.

[52] J. Anderson. *Fundamentals of Aerodynamics*. Anderson series. McGraw-Hill Education, 2010.

[53] L. Librescu and S. Na. Dynamic response of cantilevered thin-walled beams to blast and sonic-boom loadings. *Shock and Vibration*, 5(1):23–33, 1998.

[54] X. Qiu, V.S. Deshpande, and N.A. Fleck. Finite element analysis of the dynamic response of clamped sandwich beams subject to shock loading. *European Journal of Mechanics, A/Solids*, 22(6):801–814, 2003. doi : 10.1016/j.euromechsol.2003.09.002.

[55] H. Hoblit. *Gust Loads on Aircraft: Concepts and Applications*. Education Series. AIAA, Washington, USA, 1988.

[56] W. Su and C.E.S. Cesnik. Dynamic response of highly flexible flying wings. *AIAA Journal*, 49(2):324–339, 2011. doi: 10.2514/1.J050496.

[57] A. Pagani. *Component-wise models for static,dynamic and aeroelastic analyses of metallic and composite aerospace structures*. PhD thesis, Politecnico di Torino, March 2015.

[58] V. N. Shah, G. J. Bohm, and A. N. Nahavandi. Modal superposition method for computationally economical nonlinear structural analysis. *Journal of Pressure Vessel Technology*, 101:134–141, 1979. doi: 10.1115/1.3454612.

[59] R.E. Nickell. Nonlinear dynamics by mode superposition. *Computer Methods in Applied Mechanics and Engineering*, 7(1):107 – 129, 1976. doi : 10.1016/0045-7825(76)90008-6.

[60] Z. Ma and I. Hagiwara. Improved mode-superposition technique for modal frequency response analysis of coupled acoustic-structural systems. *AIAA Journal*, 29(1):1720–1726, 1991. doi: 10.2514/3.10795.

[61] T. Kant, C.P. Arora, and J.H. Varaiya. Finite element transient analysis of composite and sandwich plates based on a refined theory and a mode superposition method. *Composite Structures*, 22(2):109 – 120, 1992. doi : 10.1016/0263-8223(92)90071-J.

[62] S.R. Marur and T. Kant. On the performance of higher order theories for transient dynamic analysis of sandwich and composite beams. *Computers and Structures*, 65(5):741–759, 1997.

[63] E. Carrera, M. Petrolo, and P. Nali. Unified formulation applied to free vibrations finite element analysis of beams with arbitrary section. *Shock and Vibration*, 18(3):485–502, 2011. doi: 10.3233/SAV-2010-0528.

[64] E. Carrera and M. Petrolo. Refined beam elements with only displacement variables and plate/shell capabilities. *Meccanica*, 47(3), 2012. doi: 10.1007/s11012-011-9466-5.

[65] E. Carrera and A. Pagani. Free vibration analysis of civil engineering structures by component-wise methods. *Journal of Sound and Vibration*, 333:4597–4620, 2014. doi: 10.1016/j.jsv.2014.04.063.

[66] E. Volterra and E.C. Zachmanoglou. *Dynamics of Vibrations*. Charles E. Merill Books Inc., Ohio, USA, 1965.

[67] E. Carrera, A. Pagani, and Zangallo F. Thin-walled beams subjected to load factors and non-structural masses. *International Journal of Mechanical Sciences*, 81:109–119, 2014. doi: 10.1016/j.ijmecsci.2014.02.015.

[68] J.M. Wolff and S. Fleeter. Viscous unsteady gust aerodynamics of a flat plate airfoil by a locally analytical method. *Computers & Mathematics with Applications*, 19(6):27–36, 1990.

[69] A. Deperrois. XFLR5, 2003-2015. url : `http://www.xflr5.com/xflr5.htm`.

[70] M. Drela. Xfoil: An analysis and design system for low reynolds number airfoils. In *Low Reynolds number aerodynamics*, pages 1–12. Springer, 1989.